Article

Experimental Phase Equilibria and Isopleth Section of 8Nb-TiAl Alloys

Yong Xu [1,*], Yongfeng Liang [2], Lin Song [3], Guojian Hao [4], Bin Tian [1], Rongfu Xu [1] and Junpin Lin [2,*]

[1] School of Materials Science and Engineering, Shandong Jianzhu University, Jinan, Shandong Province, 250101, China; xuyong2612@sdjzu.edu.cn
[2] State Key Laboratory for Advanced Metals and Materials, University of Science and Technology Beijing, Beijing, 100083, China; liangyf@skl.ustb.edu.cn
[3] State Key Laboratory of Solidification Processing, Northwestern Polytechnical University, Xi'an, Shaanxi Province, 710072, China; songlin@nwpu.edu.cn
[4] Beijing Research Institute of Mechanical & Electrical Technology, Beijing, 100083, China; drhaogj@foxmail.com
* Correspondence: xuyong2612@sdjzu.edu.cn; Tel.: 86 531 8636 7286 (YX); linjunpin@skl.ustb.edu.cn; Tel.: 86 010 6233 2192 (JPL);

Abstract: The 8Nb isopleth section of a Ti-Al-Nb system is experimentally determined based on thermal analysis and thermodynamic calculation methods to obtain the phase transformation and equilibrium relations required for material design and fabrication. The phase transus and relations for the 8Nb-TiAl system show some deviations from the calculated thermodynamic results. The ordered β_o phase transforms from the disordered β/α phases at 1200–1400 °C over a large Al concentration range, and this transformation is considered to be an intermediate type between the first- and second-order phase transitions. Moreover, the β_o phases are retained at the ambient temperature in the 8Nb-TiAl microstructures. The ω_o phase transforms from the highly ordered β_o phase, rather than from α_2 or β_o with low degree of atom ordering B2 (LOB2) structure, with Al concentration of 32–43 at.% at approximately 850 °C. From the experimental detection, the transition of the ω_o phase from the β_o phase is considered to be a further ordering process.

Keywords: Titanium-Aluminum-Niobium; Phase Diagram; Vertical Section; Equilibrium Relation; CALPHAD

1. Introduction

In the past decade, TiAl-based alloys have been considered promising candidates for high-temperature materials in aerospace and automotive applications because of their excellent properties of low density, high specific yield strength and stiffness, and favorable oxidation resistance and creep properties up to high temperatures [1-3]. TiAl alloys containing high amounts of Nb, based on the γ-TiAl and α_2-Ti_3Al intermetallics, exhibit excellent high-temperature strength and oxidation resistance [4] and have attracted significant attention [3,5]. Advanced materials based on the Ti-Al-Nb alloys can be used at temperatures above 800 °C [6]. As reported by Appel et al. [3] and Erdely et al. [7], both the hot-workability and the ductility can be effectively promoted by the β phase [5,8], which provides a sufficient number of independent slip systems to act as a ductile constituent in the final microstructure [9,10]. Moreover, the solid-state transformation pathway and the microstructure of TiAl-based alloys can be manipulated through β/β_o phases [3,7,11]. According to reports by Cheng et al. [12], Kobayashi et al. [13], and Takeyama et al. [14], a multitude of solid-state transformations and resulting microstructural morphologies can be achieved by stabilizing the β phase [3].

The phase diagram and phase equilibria of Ti-Al-Nb system play important roles in material design and fabrication, especially in the manipulation of the solid-state transformation pathway and microstructure [5,15,16]. Phase transition behaviors can be precisely

Preprints (www.preprints.org) | NOT PEER-REVIEWED | Posted: 25 June 2021 doi:10.20944/preprints202106.0628.v1

detected by some thermal detection methods, such as differential scanning calorimetry (DSC), differential thermal analysis (DTA), and in-situ X-ray/neutron diffraction technologies. These determination methods generally show good agreement with each other [17-23]. Phase diagrams of the three constituent binary systems in the Ti-Al-Nb system—Ti-Al [24], Al-Nb [25] and Ti-Nb [26]—have been sufficiently delineated. The isothermal sections at 1000 °C [27-30], 1100 °C [30,31], 1150 °C [28-30], 1200 °C [27,32], 1300 °C [33], and 1400 °C [28,29,34,35], from experimental data, are available in the literature. In addition, isopleth sections show the development of phase equilibria, such as the $Ti_{72.5}Al_{27.5}$-Nb [36], $Ti_{78}Al_{22}$-Nb [37], TiAl-TiNb [37,38], 45Al [25], 47Al [25], 8Nb [25,39], and 10Nb sections [39]. Thermodynamic methods have also been adopted to assess the diagrams of Ti-Al-Nb systems [25,40,41]. Recent reviews of literatures on the Ti-Al-Nb system up to 2011 have been provided by Witusiewicz et al. [25], Cupid et al. [41], and Raghvan et al. [42]. However, insufficient experimental data contributed to some differences between these assessments, including the equilibria of the α_2, β_o, O, and ω_o phases.

The 8Nb-TiAl alloys, as a new family of TiAl-based alloys, have been widely investigated owing to the higher strength and good oxidation resistance [43,44]. For addition of 8% Nb in the TiAl alloys, the transus temperatures of α and β, as well as the α phase field, are generally decreased, inducing the significant refinement of the structure and the improvement of the yield strength [45]. However, lack of knowledge regarding the constitution of such multicomponent systems is one of the major obstacles to alloy development and significant work has to be expended to obtain reliable information on phase relationships [46]. In this work, the 8Nb isopleth section, as well as the phase equilibria, of the Ti-Al-Nb system is experimentally determined by DSC, scanning electron microscope (SEM), and X-ray diffraction (XRD). The samples were annealed sufficiently in high vacuum and then slowly cooled to achieve the equilibrium state as far as possible. However, considering the difficulty of achieving the thermodynamic equilibrium in practice, the experimental phase equilibria may have some deviations from thermodynamic equilibria. On the other hand, the experimental phase equilibria, as well as the experimental diagrams, having the treating conditions closer to the actual production, might be of great practical significance for the development and improvement of Ti-Al-Nb alloys. Table 1 presents the phases most frequently used for the Ti-Al-Nb system in this work, as well as their crystallographic data [20,41,46,47].

Table 1. Crystallographic data of phase designations occurring in this work.

Designation	Pearson	S. G. (#)	Strukt.	Prototype	Lattice Parameters (nm)		
β-Ti(Al,Nb)	*cI*2	$Im\bar{3}m$ (229)	A2	W	*a*=0.331		
α-Ti(Al,Nb)	*hP*2	$P6_3/mmc$ (194)	A3	Mg	*a*=0.295		*c*=0.468
γ-TiAl	*tP*4	$P4/mmm$ (123)	$L1_0$	AuCu	*a*=0.283		*c*=0.408
α_2-Ti_3Al	*hP*8	$P6_3/mmc$ (194)	$D0_{19}$	Ni_3Sn	*a*=0.577		*c*=0.463
β_o-TiAl(Nb)	*cP*2	$Pm\bar{3}m$ (221)	B2	CsCl	*a*=0.322		
ω_o-Ti_4NbAl_3	*hP*6	$P6_3/mmc$ (194)	$B8_2$	$InNi_2$	*a*=0.458		*c*=0.552
O-Ti_2NbAl	*oC*16	$Cmcm$ (63)	---	NaHg	*a*=0.616	*b*=0.973	*c*=0.470

2. Materials and Methods

Eighteen ternary 8Nb-TiAl alloy buttons were prepared by non-consumable arc melting (with a tungsten electrode) from high-purity initial components (Ti, Al, Nb: 99.99 wt. %), using a water-cooled copper hearth in an ultra-high-purity argon atmosphere. Only those samples with less than 1.0 wt.% weight losses were adopted for further analysis. Hereafter, all compositions are presented in atomic percentage (at. %), unless declared otherwise. Each button (with a mass of approximately 30 g) was melted, turned over, and re-melted five times to ensure homogeneity. The diffusion annealing was performed in high vacuum at 1400 °C for 20 hours to equilibrate and coarsen the phase. The samples were then slowly cooled to 50 °C in the furnace (cooling rate: ~1.0 °C/min). Thermodynamic equilibrium calculations were performed by the Calculation Phase Diagrams (CALPHAD) method using the commercial software Pandat© [48], following the thermodynamic description from Witusiewicz's investigation [25]. The phase structures were detected by XRD using powder samples on a Bruker D8 Advance, operated at 40 kV and 40 mA with Cu Kα. For the morphology analysis, sample sizes of 8 mm × 8 mm × 8 mm were cut from the centers of the buttons with an electron discharge cutting machine, and the samples were then polished following standard mechanical polishing procedures. The microstructures of the annealed samples were obtained by SEM in back-scattered electron (BSE) mode (JEOL JSM-6380), operated at 20 kV and at a working distance of 10 mm. The compositions in the samples were analyzed by the electron probe microanalysis (EPMA) on JEOL JXA-8530F Plus and the optical emission spectrometer (OES) on Bruker Q4 TASMAN 130. The composition of a given phase was detected by EPMA from at least 12 points to acquire a mean value. The impurities had mass contents of less than 150 ppm nitrogen and of less than 380 ppm oxygen.

The solid-state transformation temperatures were determined by DSC on a NETZSCH DSC 404 C with an Al_2O_3 crucible. Discs of 4 mm diameter and 3 mm thickness (150–180 mg), which produced sufficient signals in the argon atmosphere, were machined from the centers of the buttons. Temperature calibrations for the equipment were conducted by melting high-purity Cu, Al, Ag, and Ni at scan rates of 5 and 10 °C/min to determine the correction equation. In this work, the heating rate for all test samples (excluding the calibration samples) was 10 °C/min, using a covered Al_2O_3 crucible with a maximum temperature of 1450 °C, and within a dynamic Ar atmosphere with a flow rate of 30 mL/min. To account for the influence of the containers, the DSC signals of the empty crucibles were subtracted from the detected traces. As a standard comparison sample, thermal data were acquired from sapphire, using the same parameters as those applied to the 8Nb-TiAl samples, to determine the specific heat capacity (C_p) by Eq. (1).

$$C_p^{Sample} = \frac{DSC_{sample}}{DSC_{sapphire}} \cdot C_p^{Sapphire} \quad (1)$$

In this work, to improve the accuracy and uniformity of the data acquisition process, a new method was developed for determining and calibrating the onset transformation temperatures for the different cooling/heating rates in DSC detection. The first derivatives of the DSC traces (DDSC) were employed to determine the transformation temperatures. The temperature difference, ΔT=38 °C, was adopted to calibrate the dynamic transformation temperatures.

3. Results

3.1. Phase Evolution

The nominal compositions of the 8Nb-TiAl alloys (sample numbers S01–S18) and the compositions of the individual phases determined by EPMA/OES/XRD are presented in Table 2. The specific reflections of certain phases—α_2(202), γ(002)/(200), O(310), and β_o(200)/ω_o(202)—were selected to describe the phase evolution, as shown in Figure 1(a). The reflection in S01 at approximately 38.5° was much stronger than the reflection at 40.8°, showing the overlap of the diffraction peaks with the β_o phase. For this β_o phase, the (110)/(220) reflections of disordered β structure were preserved, whereas the (200)/(211) reflections were suppressed, indicating a LOB2 structure, as shown in Figure 1(b). However, as shown by the XRD pattern of Sample S06, the reflection at approximately 39.3° was considered to indicate overlapping of the β_o and ω_o phases, as shown in Figure 1(b).

The evolution of the fraction of each phase in the samples can be roughly evaluated by the reflection peak height, where unstacked reflections should be selected first. Figure 2 shows the peaks of the α_2(202), γ(002)/(200), O(310), and β_o(200)/ω_o(202) reflections in the 8Nb-TiAl samples. The α_2 phase was detected as the main phase in all the samples, as shown in Figure 1. The fraction of α_2 phase increased with increased Al content in Samples S01–S10, then decreased with continuing Al increases in Samples S11–S18, as shown in Figure 2(a). The fraction of γ phase was small in Samples S01–S10, and then the γ phase fraction increased continuously as the Al content increased in Samples S11–S18, as shown in Figure 2(c). The presence of O phase could be identified by the (310) reflection in the

Preprints (www.preprints.org) | NOT PEER-REVIEWED | Posted: 25 June 2021 doi:10.20944/preprints202106.0628.v1

Al-lean S01–S05 samples, as shown in Figure 2(b), and the ω_o and β_o phases were identified in Samples S06–S12, as shown in Figure 1(b) and Figure 2(d). The fraction of β_o+ω_o phases increased dramatically in Samples S06–S09, then decreased in S10–S13. In the Al-rich S13–S18 samples, only two phases formed: α_2 and γ.

Table 2. Nominal and determined compositions (at. %) of the 8Nb-TiAl alloys.

Sample	Nominal Composition	Chemical Composition (OES)		
		Al	Ti	Nb
S01	$Ti_{73.6}Al_{18.4}Nb_8$	18.34	73.69	7.97
S02	$Ti_{70.8}Al_{21.2}Nb_8$	21.13	70.89	7.98
S03	$Ti_{68.1}Al_{23.9}Nb_8$	23.80	68.23	7.97
S04	$Ti_{65.3}Al_{26.7}Nb_8$	26.65	65.37	7.98
S05	$Ti_{62.6}Al_{29.4}Nb_8$	29.37	62.66	7.97
S06	$Ti_{59.8}Al_{32.2}Nb_8$	32.16	59.87	7.97
S07	$Ti_{58.4}Al_{33.6}Nb_8$	33.52	58.51	7.97
S08	$Ti_{57.0}Al_{35.0}Nb_8$	34.89	57.11	8.00
S09	$Ti_{55.7}Al_{36.3}Nb_8$	36.24	55.75	8.01
S10	$Ti_{54.3}Al_{37.7}Nb_8$	37.63	54.35	8.02
S11	$Ti_{52.9}Al_{39.1}Nb_8$	39.01	52.96	8.03
S12	$Ti_{51.5}Al_{40.5}Nb_8$	40.42	51.56	8.02
S13	$Ti_{50.1}Al_{41.9}Nb_8$	41.83	50.14	8.03
S14	$Ti_{48.8}Al_{43.2}Nb_8$	43.13	48.84	8.03
S15	$Ti_{47.4}Al_{44.6}Nb_8$	44.53	47.44	8.03
S16	$Ti_{46.0}Al_{46.0}Nb_8$	45.93	46.04	8.03
S17	$Ti_{44.6}Al_{47.4}Nb_8$	47.35	44.63	8.02
S18	$Ti_{43.2}Al_{48.8}Nb_8$	48.72	43.27	8.01

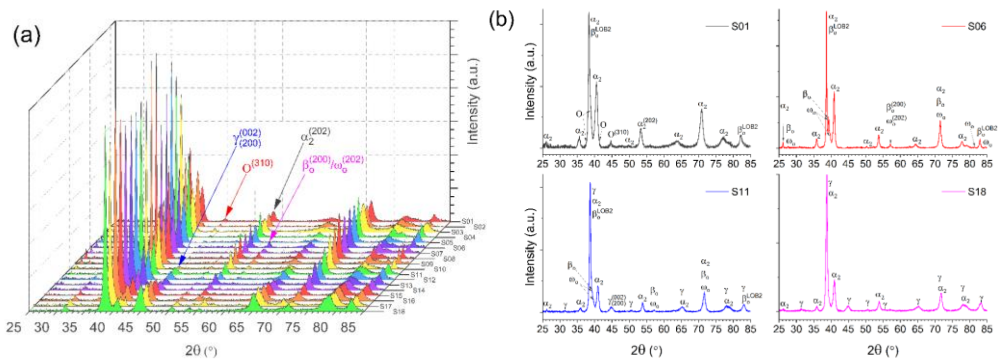

Figure 1. XRD detection of (a) tracking patterns for Samples S01–S18 and (b) single pattern of several selected samples.

Preprints (www.preprints.org) | NOT PEER-REVIEWED | Posted: 25 June 2021 doi:10.20944/preprints202106.0628.v1

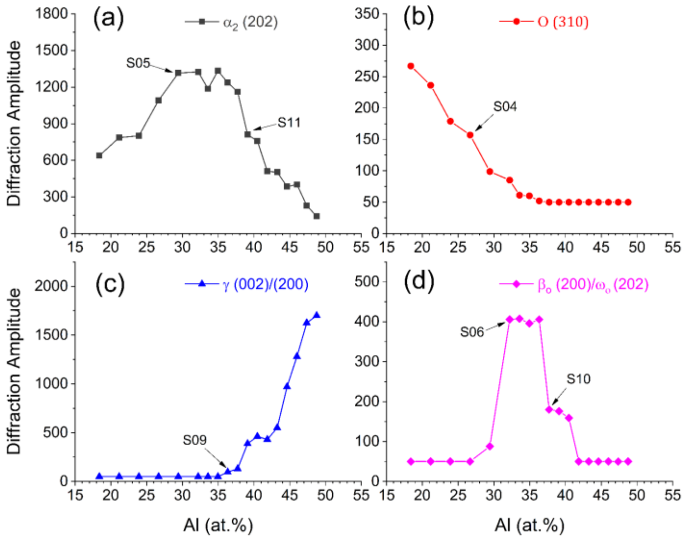

Figure 2. Phase evolution in 8Nb-TiAl alloys, determined by the reflection peak height of the (a) α_2 (202), (b) O (310), (c) γ (002)/(200), and (d) β_o (200)/ω_o (202) crystal planes.

3.2. Morphology

As shown in Figure 3(a,b), the morphologies of Samples S01–S05 (18.4–29.4% Al) comprised coarse α_2 laths and O phase (dark regions); flaky α_2 particles in the low order β_o matrix; interwoven β_o structures (bright regions). The β_o phase mainly appeared along the α_2 grain boundaries and only a small volume fraction of the β_o phase was present within the α_2 laths. As Al increased in Samples S01–S05, the fraction of α_2 increased while the O and β_o phases decreased, as observed by the morphology analysis. The presence of ω_o in Samples S06–S12 was identified by XRD, as shown in Figure 1, whereas this phase was not observed in the microstructure, as shown in Figs. 3 and 4. For Samples S06–S09, the morphology mainly consisted of the coarse α_2 laths and interwoven β_o+ω_o structures, as shown in Figure 3(c,d). The β_o phase was mainly located along colony boundaries and only a small volume fraction was present within the colonies [5]. The morphologies of Samples S10–S12 consisted of lamellar colonies, $(\alpha_2+\gamma)_L$, and interwoven β_o+ω_o structures, as shown in Figure 3(e,f). Isolated γ equiaxed grains were found on the boundaries of α_2 and β_o, as shown in Figs. 3 and 4. The morphologies of Samples S13–S17 were fully lamellar, as shown in Figure 4(a-d). The size of the lamellar colonies and the interlamellar spacing in these samples increased greatly. Figure 4(c,d) shows that both the proeutectoid α_2 and the γ were largely situated along boundaries, at the triple lines of $(\alpha_2+\gamma)_L$, and around the β_o grains. However, the presence of β_o and γ was extremely restrained as the Al content increased to 44.6%, as shown in Figure 4(c,d). The morphology of Sample S18 consisted of coarse γ laths and interwoven eutectoid α_2+γ microstructures, as shown in Figure 4(e,f).

3.3. Thermal Analysis

The phase transformation temperatures of 8Nb-TiAl alloys during experimental continuous heating were determined by thermal analysis. The phase transitions were simultaneously determined by DSC and C_p data, with the calculated C_p for comparison. Figure 5 shows the thermodynamically calculated C_p data and experimentally determined DSC and C_p data for the selected samples. The abrupt changes in the calculated C_p, shown by the narrow peaks in Figure 5(a), correspond to the formation of an ordered β_o phase from α/β; the order-disorder transitions of $\beta\leftrightarrow\beta_o$ and the eutectoid reaction of $\alpha\leftrightarrow\beta_o+\gamma$ can also be determined from the experimental C_p data, as shown in Figure 5(b,c). However, as shown in Figure 5(c), there is a particularly broad peak at approximately 900 °C in the experimental C_p curve, indicating an additional ordering transition in Samples S06–S12,

Preprints (www.preprints.org) | NOT PEER-REVIEWED | Posted: 25 June 2021 doi:10.20944/preprints202106.0628.v1

which was considered to be the $\beta_o \leftrightarrow \omega_o$ transition. For Samples S15–S18, no $\beta \leftrightarrow \beta_o$ transition was found at elevated temperatures, as shown in Figure 5(d). Based on the DSC, SEM, and XRD analyses, the phase transitions in 8Nb-TiAl alloys were determined, as shown in Figure 5(b-d), where the phase regions and isopleth sections are schematically identified in the DSC/C_p curves.

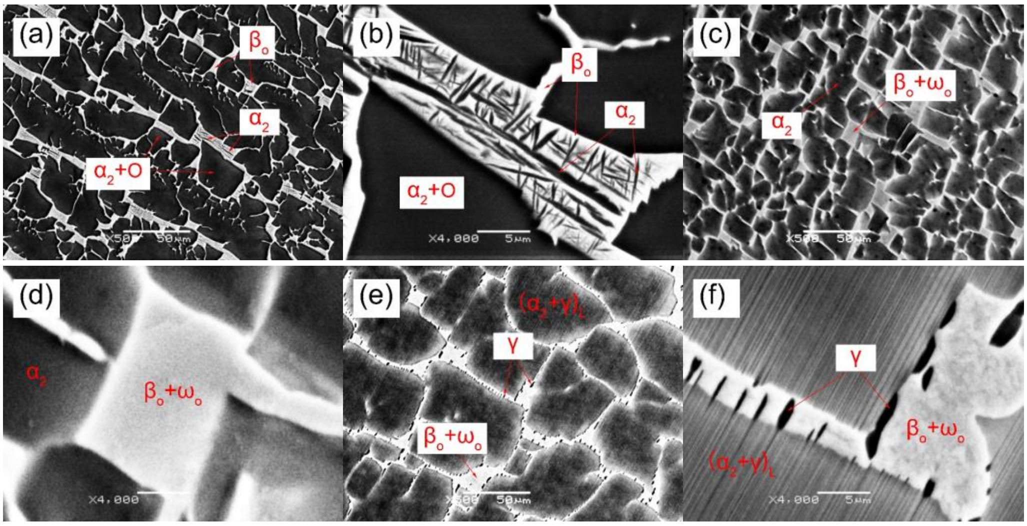

Figure 3. Microstructures (from SEM-BSE) of Samples (a-b) S01, (c-d) S06, and (e-f) S11.

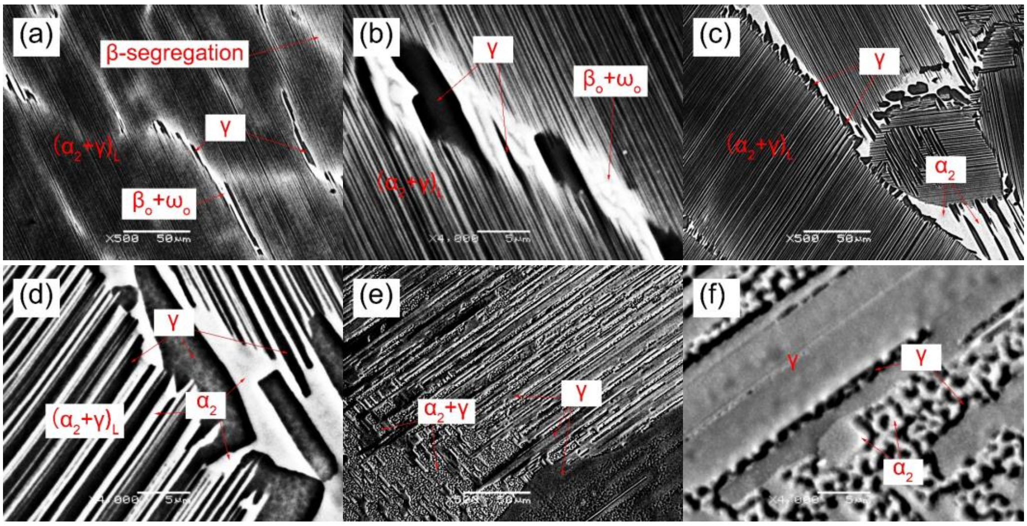

Figure 4. Microstructures (from SEM-BSE) of Samples (a-b) S13, (c-d) S15, and (e-f) S18.

3.4. Isopleth

Based on this work's thermal analyses, the experimental 8Nb-TiAl isopleth section was deduced and compared with a thermodynamic isopleth, as shown in Figure 6. The experimental transus between phase transitions was approximated by a three-order polynomial with a least-squares solution, as shown in Figure 6. The experimental isopleth showed some differences from the thermodynamic calculations.

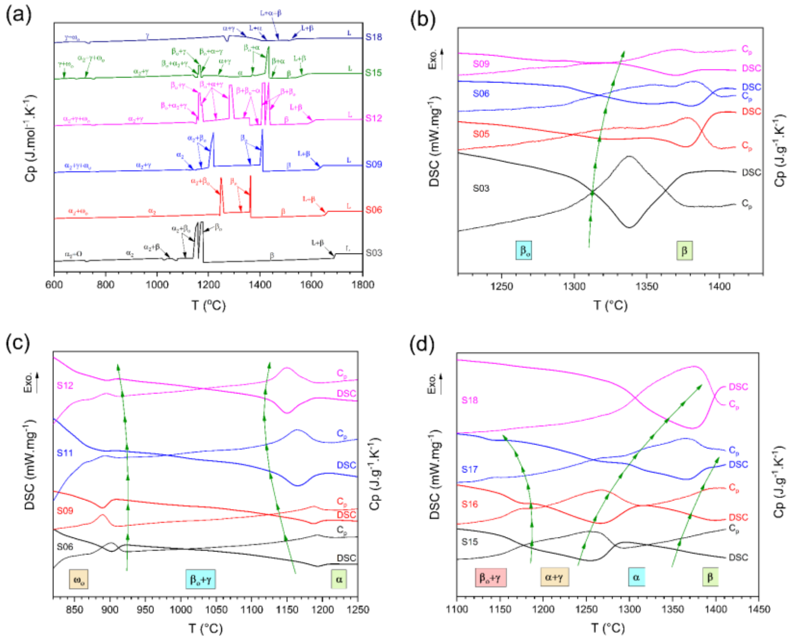

Figure 5. Thermal analysis of 8Nb-TiAl: (a) calculated C_p and (b-d) experimentally determined DSC and C_p data. The phase regions are demarcated by the arrows based on the experimental isopleth.

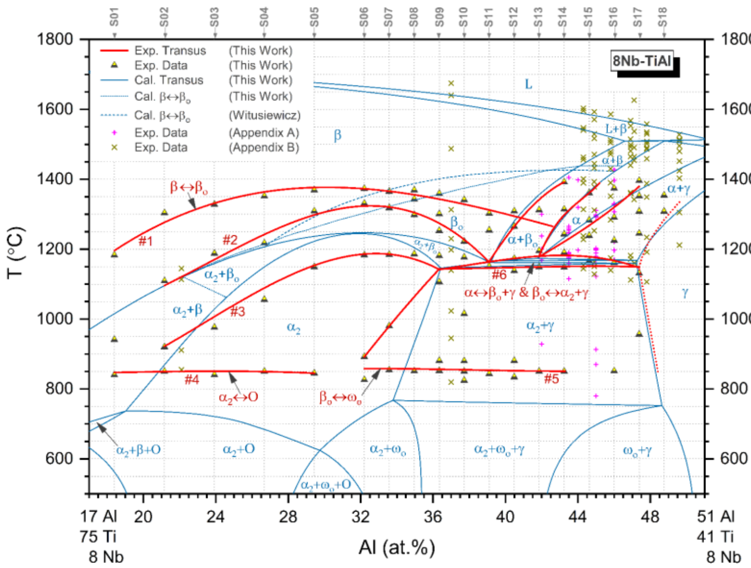

Figure 6. Isopleth of 8Nb-TiAl ternary system. The diagram calculated by CALPHAD is shown by the thin solid lines. The $\beta\leftrightarrow\beta_o$ transition are labeled as the short dot lines for calculated data in this work, and the double dot dash lines from Witusiewicz's investigation [25]. The onset transformation temperatures detected by DSC are marked as the half-filled triangles, while as the crosses for the experimental data from literatures. The experimental transus, marked as the solid lines (#1-6). The boundaries of γ single phase are estimated by calculation data, plotted as the dot lines.

The phase transition behaviors found in this work were in good agreement with those previously reported in the literature, as shown in Figure 6. Schmoelzer et al. [11] and Erdely et al. [7] determined the phase transition temperatures in Ti-43.5Al-(4-5)Nb-(Mo, B) alloys using DSC and in-situ high-energy X-ray diffraction (HEXRD) methods. The eutectoid transition ($\alpha\leftrightarrow\beta_o+\gamma$ and $\beta_o\leftrightarrow\alpha_2+\gamma$) temperature has been considered to be T_{eut} = 1160–1180 °C, whereas the $\alpha\leftrightarrow\gamma$ temperature has been T_α =1246–1255 °C; these results agreed well with the transition temperatures taken from the experimental transus, T_{eut} = 1151–1178 °C and T_α = 1230 °C, respectively. The order-disorder $\beta\leftrightarrow\beta_o$ transition temperatures have been detected at 1225 °C for Ti-43.5Al-4Nb-(Mo, B) [7,11], and 1200 °C

 doi:10.20944/preprints202106.0628.v1

for Ti-(42-43.5)Al-Nb [7,17], in agreement with the transus temperature, 1250–1270 °C in the experimental isopleth, as shown in Figure 6. The $\alpha \leftrightarrow \alpha_2+\gamma$ transformation temperatures in Ti-(42-43.5)Al-Nb have been detected at 1169 °C by in-situ HEXRD and DSC [7,17], located exactly in the phase regions of the experimental isopleth. Meanwhile, the $\alpha \leftrightarrow \beta$ transition temperature has been considered to be approximately 1300 °C [17], corresponding to the experimental value, approximately 1310 °C, in the isopleth. For the Ti-45Al-8.5Nb-(W,B,Y) alloy [49], the $\alpha \leftrightarrow \gamma$ and eutectoid transition temperatures have been considered to be in the range of 1150–1310 °C and 1100–1220 °C, and these were determined to be 1280 °C and 1150–1176 °C in the experimental isopleth, respectively.

The $\beta_o \leftrightarrow \omega_o$ transition temperatures in Ti-45Al-10Nb have been determined to be approximately 780 °C with a slow cooling process (10 °C/min), and approximately 850–870 °C with a heating process (10 °C/min) [20,50]. In addition, during a slow furnace cooling process, the $\beta_o \leftrightarrow \omega_o$ transition temperature in Ti-42Al-8.5Nb has been detected at 928 °C by in-situ HEXRD and DSC with a heating rate of 20 °C/min [17]. These experimental results are in good agreement with the transus determined in this work. In contrast, at the temperatures near 800 °C, the $\alpha_2 \leftrightarrow \omega_o$ transition has been seen to occur in only a few minutes with applied stress, although the transition took several hundred hours without applied stress [51]. Moreover, the $\beta_o \leftrightarrow \omega_o$ transition is promoted by the addition of a β/β_o-stabilizing element, such as Nb or Mo [20,25,52,53]. The $\alpha_2 \leftrightarrow \omega_o$ transition has been observed to be restrained by the addition of an α_2-stabilizing element, such as C [51].

4. Discussion

4.1. Phase Equilibria

As shown in Figure 6, the experimental 8Nb-TiAl alloys exhibited the transformation pathway $\beta \rightarrow \beta+\beta_o \rightarrow \beta_o+\alpha_2 \rightarrow \beta_o+\alpha_2+O$ for Al concentrations lower than 30%, and $\beta \rightarrow \beta+\beta_o \rightarrow \beta_o+\alpha_2 \rightarrow \beta_o+\alpha_2+\gamma \rightarrow \beta_o+\omega_o+\alpha_2+\gamma$ for Al concentrations of 30–39%. The eutectoid transitions, $\alpha \leftrightarrow \beta_o+\gamma$ and $\beta_o \leftrightarrow \alpha_2+\gamma$, as well as the $\beta_o \leftrightarrow \gamma$ transition, had to be considered a single region in this work because of the lack of sufficient experimental data. For alloys with 39–42% Al, a pathway with the α phase emerged, $\beta \rightarrow \beta+\beta_o/\alpha \rightarrow \beta+\beta_o+\alpha \rightarrow \beta+\beta_o+\alpha+\gamma \rightarrow \beta_o+\omega_o+\alpha_2+\gamma$. For alloys with 42–47% Al, the pathway was $\beta \rightarrow \beta+\alpha \rightarrow \alpha \rightarrow \alpha+\gamma \rightarrow \alpha+\beta_o+\alpha_2+\gamma \rightarrow \alpha_2+\gamma$. For alloys with Al concentrations greater than 47%, the pathway was $\beta+\alpha \rightarrow \alpha \rightarrow \alpha+\gamma \rightarrow \alpha_2+\gamma$.

In the 8Nb-TiAl system, the $\beta \leftrightarrow \beta_o$ transition occurred over a large range of Al concentrations, as shown in Figure 6. The transitions of samples with Al ranges of 18.4–43.2% at 1200–1400 °C, indicated by the #1 transus line in Figure 6, exhibited higher transformation temperatures than those calculated, which increased as the Al concentration became lower than 33.5%, with a maximum transformation temperature of 1380 °C at 32% Al. While the transition temperature decreased over the range of 33.5–42.5% Al and disappeared entirely as the Al concentration increased above 44.0% Al.

For alloys with 18–36% Al, following the $\beta \leftrightarrow \beta_o$ transus, there was a high-temperature phase transition, determined as the ordered α_2 phase transformation from β_o phases (the #2 and #3 transus lines in the isopleth), as shown in Figure 6. The preliminary α_2 phase formed the coarsening laths among the β_o phase, and subsequent α_2 phase forms the flaky particles in the β_o matrix, as shown in Figure 1.

For alloys with 18–30% Al, the formation of O phase was determined by XRD, although not observed in the microstructures because of the small amount of the phase fraction in the alloy matrix, as shown in Figure 1. The fraction of O phase in the samples decreased and the α_2 phase increased as the Al concentration increased, as shown in Figure 2(c,d). The O phase can be formed in a large temperature range between 800–1000 °C in Ti-Al-Nb ternary alloys [54,55], with two different pathways in the Ti-Al-Nb ternary system—$\alpha_2 \leftrightarrow O$ and $\beta_o \leftrightarrow O$—depending on the composition and treatment process [17,56]. One pathway occurs in the α_2 phase in low-Nb-containing TiAl alloys (≤12.5% Nb), and the other pathway occurs in the β_o phase in high-Nb-containing alloys (~25% Nb)

Preprints (www.preprints.org) | NOT PEER-REVIEWED | Posted: 25 June 2021 doi:10.20944/preprints202106.0628.v1

[17,56,57]. The transformation of the O phase from the β_o phase is considered to occur through a martensitic transition [57]. Therefore, in this work, the transus line in the range of 18–30% Al at approximately 850 °C in the 8Nb-TiAl system was confirmed to be the $\alpha_2 \leftrightarrow$O transition, in agreement with the thermodynamic calculation.

For alloys with 32–36% Al, there was an extra γ precipitation from α_2, forming the ultrafine lamellar structure. As the Al concentration increased above 36%, the lamellar structure mainly formed through eutectoid reactions at 1150–1200 °C, with $\alpha \leftrightarrow \beta_o+\gamma$ and $\beta_o \leftrightarrow \alpha_2+\gamma$, forming the lamellar colonies as shown in Figs. 3–4 and 6. Therefore, as mentioned in the thermal analysis, the experimental phase transformation behaviors within α-containing regions were in good agreement with the thermodynamic calculations, as shown in Figure 5(a,b,d), indicating that the influence of experimental conditions on these regions is small. The dominant activity under these conditions is suggested to be the main attribution.

For alloys with Al concentrations lower than 30% (Samples S01–S05) or greater than 43% (Samples S14–S18), there were no β_o (LOB2 structure) and ω_o phases found at the ambient temperature, as indicated by XRD and SEM detections. While for Al concentrations in the range of 32–42% (Samples S06–S12), the ω_o phase and highly ordered β_o phase were detected simultaneously. As a result, the ω_o phase was preferentially formed in the highly ordered β_o phase.

The experimental phase equilibrium relations and transformation pathways of the 8Nb-TiAl alloys deviated significantly from the thermodynamic calculations, as shown in Figure 6. These deviations may have been associated with the treatment conditions, such as the heating / cooling rates, and / or insufficiencies in the thermodynamic database for high-Nb-containing TiAl systems [5,11,58]. Because of the actual preparation process, the experimental isopleth showed metastable phase behavior, such as the formation of ω_o from the retained β_o, rather than from α_2 as expected by the thermodynamic equilibrium behavior.

4.2. *β_o Transformation*

The $\beta \leftrightarrow \beta_o$ transition temperatures and ordering procedure were in agreement with the studies of Clemens et al. [5] and Schmoelzer et al. [11], and were strongly affected by the compositions, as in [11,25]. The transition temperature differences between the experimental and calculation results may also have been related to the ordering of the β phase [59]. Crystallographic analysis has shown that the structure of the ordered β_o phase contains two sublattices: one occupied by Al (B site) and the other occupied by Ti atoms (A site). The two sublattices are randomly occupied with all species in the disordered β phase. As previously reported [60], Nb atoms should replace the Ti atoms in the structure. However, Leonard et al. [61] suggested that the site occupancy of Nb depends on the composition. The atomic occupancy and lattice parameter are slightly changed during the $\beta \leftrightarrow \beta_o$ order-disorder transition.

The phase transition type is evidently reliant on the order of the isobaric-isothermal potential derivative (free Gibbs energy) [62], which exhibits an abrupt change at the transition position. In the first-order phase transitions (first derivatives), determined by the heat release or endothermic peaks in the DSC curve, there are abrupt changes in the specific volume and entropy. In the second-order phase transitions, such as order-disorder transitions, there are continuous changes in the specific volume and entropy, with no transition heat shown in the DSC curve, although there are abrupt changes in the second derivatives of the isobaric-isothermal potential, such as in the specific heat capacity, thermal expansion coefficient, and isothermal compressibility [62].

In this work, the ordered β_o phase formed from disordered β/α phases as the temperature decreased from the elevated temperatures. As mentioned in reference to the calculated C_p patterns, shown in Figure 5(a), there was one narrow peak in Sample S03, indicating the order-disorder $\beta \leftrightarrow \beta_o$ transition, and there were two narrow peaks in Samples S06–S15, corresponding to two types of order-disorder transitions, $\beta \leftrightarrow \beta_o$ and $\alpha \leftrightarrow \beta_o+\gamma$.

Preprints (www.preprints.org) | NOT PEER-REVIEWED | Posted: 25 June 2021 doi:10.20944/preprints202106.0628.v1

The thermal analysis unambiguously detected the transformations of β_o from β/α, as shown in Figure 5(b,d); these transformations are commonly considered second-order phase transitions. However, in addition to the peaks found in the C_P patterns, endothermic peaks were also detected in the DSC patterns for $\beta \leftrightarrow \beta_o$ and $\alpha \leftrightarrow \beta_o+\gamma$ transitions, as shown in Figure 5(b,d), indicating that the order-disorder transitions, $\beta \leftrightarrow \beta_o$ and $\alpha \leftrightarrow \beta_o+\gamma$, in the 8Nb-TiAl system should be defined as an intermediate transition type, between the first- and second-order phase transitions.

4.3. ω_o Transformation

The transformation of β_o phase to ω_o phase in Nb-containing TiAl alloys at 700–900 °C has been frequently observed [20,63-65]. The ω_o phase has been found to be transformed within the β_o matrix by homogeneous nucleation, or on the boundaries of β_o/γ phases by heterogeneous nucleation, of particles with nano- or micro-scale sizes during continuous heating/cooling processes [17,20,51,65]. The formation of ω_o phase is associated closely with the treatment process [51,66] and the chemical composition [20], and Nb has been suggested to act as the ω_o stabilization element [67].

As shown in Figure 5(c), there was an endothermic peak and an abrupt change in the DSC and C_P patterns, respectively, indicating that, to some extent, the $\beta_o \leftrightarrow \omega_o$ transition was an ordering process. As mentioned by Stark et al. [20], the β_o phase exhibits a crystallographic orientation with the ω_o phase: $\{111\}\beta_o \parallel \{0001\}\omega_o$ or $\langle 1\bar{1}0\rangle\beta_o \parallel \langle 11\bar{2}0\rangle\omega_o$. According to this relationship, Figure 7 shows the atomic configuration of the ω_o phase with the Wyckoff positions and site occupancies, as well as the atom distribution in β_o phase as seen along its 3-fold axis. During the $\beta_o \rightarrow \omega_o$ transformation, the four stacking atomic layers in the β_o phase, Layers 1–4 in Figure 7(a), merge into double layers in the ω_o phase, Layers 1–2 in Figure 7(b). Furthermore, the site occupancy preference also changed, such that the Nb atoms moved into the 2a site, whereas the Ti and Al atoms move almost into the 2c and 2d sites, as shown in Figure 7. The lattice of the ω_o phase is slightly compressed along the $\langle 111\rangle\beta_o/\langle 0001\rangle\omega_o$ direction, whereas it stretches significantly along the $\langle 1120\rangle\omega_o$ direction [20].

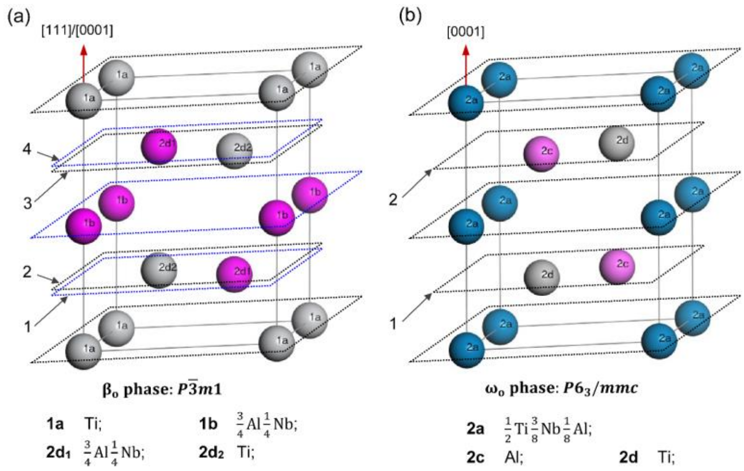

Figure 7. Atomic configurations of (a) β_o and (b) ω_o structures. Wyckoff positions and site occupancies [20] are given at bottom.

5. Conclusions

(1) The isopleth section of the 8Nb-TiAl system (with 18–48% Al) was determined experimentally by DSC, SEM, and XRD methods, and compared with thermodynamic calculations (from CALPHAD). The experimental isopleth showed some deviations from the calculations, especially for β_o containing regions.

(2) The ordered β_o phase transformed from the disordered β phase in the range of 18.4–43.2% Al at 1200–1400 °C. The β_o phase also transformed through a eutectoid transition, $\alpha \leftrightarrow \beta_o+\gamma$, from the α phase. The transition type of $\beta \leftrightarrow \beta_o$ was considered to be an

intermediate type between the first- and second-order phase transitions. In particular, the β_o phases were retained at the ambient temperature in the 8Nb-TiAl alloys under experimental conditions.

(3) The ordered ω_o phase transformed experimentally from the highly ordered β_o phase rather than from the α_2 phase or the β_o phase with a LOB2 structure. The experimentally detected ω_o formation occurred within 32–43% Al concentrations at approximately 850 °C, having a smaller composition range and higher transforming temperature than the calculated thermodynamic transition. The formation of the ω_o phase from the β_o phase was considered to be a further ordering process.

6. Patents

This section is not mandatory but may be added if there are patents resulting from the work reported in this manuscript.

Supplementary Materials: The following are available online at www.mdpi.com/xxx/s1, Figure S1: DSC and DDSC traces for samples that are closed to invariant points. Table S1: Onset phase transformation temperatures detected by thermal analysis. Table S2: DSC/DTA data for detecting the phase transition temperatures in the Ti-Al-Nb samples from the literatures. Table S3: Experimental transition temperatures in the Ti-Al-Nb samples summarized by Witusiewicz et al.

Author Contributions: Conceptualization, Y.X. and Y.F.L.; methodology, L.S.; software, Y.X. and B.T.; validation, Y.X. and J.P.L.; formal analysis, Y.X.; investigation, Y.F.L. and R.F.X.; resources, G.J.H.; data curation, Y.X.; writing—original draft preparation, Y.X.; writing—review and editing, J.P.L.; visualization, B.T.; supervision, J.P.L.; project administration, Y.X. and J.P.L.; funding acquisition, Y.F.L., L.S. and J.P.L. All authors have read and agreed to the published version of the manuscript.

Acknowledgments: This research was supported by the National Natural Science Foundation of China (Nos. 51831001 and 51971175), Funds for Creative Research Groups of China (51921001), Fundamental Research Funds for the Central Universities (FRF-MP-20-44), the State Key Lab of Advanced Metals and Materials (2018-ZD05) and the Fundamental Research Funds of Shandong University (2018JCG05).

Conflicts of Interest: The authors declare no conflict of interest.

References

1. Clemens, H.; Kestler, H. Processing and Applications of Intermetallic γ-TiAl-Based Alloys. *Advanced Engineering Materials* **2000**, *2*, 551-570.
2. Kim, Y.-W.; Dimiduk, D. Progress in the understanding of gamma titanium aluminides. *JOM* **1991**, *43*, 40-47.
3. Appel, F.; Oehring, M.; Paul, J.D.H. Nano-Scale Design of TiAl Alloys Based on β-Phase Decomposition. *Advanced Engineering Materials* **2006**, *8*, 371-376.
4. Appel, F.; Wagner, R. Microstructure and deformation of two-phase γ-titanium aluminides. *Materials Science and Engineering: R* **1998**, *22*, 187-268.
5. Clemens, H.; Wallgram, W.; Kremmer, S.; Güther, V.; Otto, A.; Bartels, A. Design of Novel β-Solidifying TiAl Alloys with Adjustable β/B2-Phase Fraction and Excellent Hot-Workability. *Advanced Engineering Materials* **2008**, *10*, 707-713.
6. Hoelzer, D.T.; Ebrahimi, F. Phase Stability of Sigma + Beta Microstructures in the Ternary Nb-Ti-Al System. *MRS Proceedings* **1990**, *194*, 393.
7. Erdely, P.; Werner, R.; Schwaighofer, E.; Clemens, H.; Mayer, S. In-situ study of the time–temperature-transformation behaviour of a multi-phase intermetallic β-stabilised TiAl alloy. *Intermetallics* **2015**, *57*, 17-24.
8. Wallgram, W.; Schmölzer, T.; Cha, L.; Das, G.; Güther, V.; Clemens, H. Technology and mechanical properties of advanced γ-TiAl based alloys. *International Journal of Materials Research* **2009**, *100*, 1021-1030.
9. Liss, K.-D.; Schmoelzer, T.; Yan, K.; Reid, M.; Peel, M.; Dippenaar, R.; Clemens, H. In situ study of dynamic recrystallization and hot deformation behavior of a multiphase titanium aluminide alloy. *Journal of Applied Physics* **2009**, *106*, 113526.
10. Tetsui, T.; Shindo, K.; Kaji, S.; Kobayashi, S.; Takeyama, M. Fabrication of TiAl components by means of hot forging and machining. *Intermetallics* **2005**, *13*, 971-978.
11. Schmoelzer, T.; Liss, K.-D.; Zickler, G.A.; Watson, I.J.; Droessler, L.M.; Wallgram, W.; Buslaps, T.; Studer, A.; Clemens, H. Phase fractions, transition and ordering temperatures in TiAl–Nb–Mo alloys: An in- and ex-situ study. *Intermetallics* **2010**, *18*, 1544-1552.
12. Cheng, T.T.; Loretto, M.H. The decomposition of the beta phase in Ti–44Al–8Nb and Ti–44Al–4Nb–4Zr–0.2Si alloys. *Acta Materialia* **1998**, *46*, 4801-4819.

13. Kobayashi, S.; Takeyama, M.; Motegi, T.; Hirota, N.; Matsuo, T. Formation of β-Ti Phase in Multi-component Gamma Alloys. *MRS Proceedings* **2002**, *753*, BB3.4.
14. Takeyama, M.; Kobayashi, S. Physical metallurgy for wrought gamma titanium aluminides: Microstructure control through phase transformations. *Intermetallics* **2005**, *13*, 993-999.
15. Tetsui, T.; Shindo, K.; Kobayashi, S.; Takeyama, M. A newly developed hot worked TiAl alloy for blades and structural components. *Scripta Materialia* **2002**, *47*, 399-403.
16. Huber, D.; Clemens, H.; Stockinger, M. Near Conventional Forging of an Advanced TiAl Alloy. *MRS Proceedings* **2012**, *1516*, 23-28.
17. Rackel, M.W.; Stark, A.; Gabrisch, H.; Schell, N.; Schreyer, A.; Pyczak, F. Orthorhombic phase formation in a Nb-rich γ-TiAl based alloy – An in situ synchrotron radiation investigation. *Acta Materialia* **2016**, *121*, 343-351.
18. Sun, P.; Fang, Z.Z.; Koopman, M.; Paramore, J.; Chandran, K.S.R.; Ren, Y.; Lu, J. An experimental study of the (Ti–6Al–4V)–xH phase diagram using in situ synchrotron XRD and TGA/DSC techniques. *Acta Materialia* **2015**, *84*, 29-41.
19. Šmilauerová, J.; Harcuba, P.; Kriegner, D.; Janeček, M.; Holý, V. Growth kinetics of ω particles in β-Ti matrix studied by in situ small-angle X-ray scattering. *Acta Materialia* **2015**, *100*, 126-134.
20. Stark, A.; Oehring, M.; Pyczak, F.; Schreyer, A. In Situ Observation of Various Phase Transformation Paths in Nb-Rich TiAl Alloys during Quenching with Different Rates. *Advanced Engineering Materials* **2011**, *13*, 700-704.
21. Clemens, H.; Chladil, H.F.; Wallgram, W.; Zickler, G.A.; Gerling, R.; Liss, K.D.; Kremmer, S.; Güther, V.; Smarsly, W. In and ex situ investigations of the β-phase in a Nb and Mo containing γ-TiAl based alloy. *Intermetallics* **2008**, *16*, 827-833.
22. Appel, F.; Oehring, M.; Paul, J.D.H. A novel in situ composite structure in TiAl alloys. *Materials Science and Engineering: A* **2008**, *493*, 232-236.
23. Liss, K.-D.; Bartels, A.; Clemens, H.; Bystrzanowski, S.; Stark, A.; Buslaps, T.; Schimansky, F.-P.; Gerling, R.; Scheu, C.; Schreyer, A. Recrystallization and phase transitions in a γ-TiAl-based alloy as observed by ex situ and in situ high-energy X-ray diffraction. *Acta Materialia* **2006**, *54*, 3721-3735.
24. Ohnuma, I.; Fujita, Y.; Mitsui, H.; Ishikawa, K.; Kainuma, R.; Ishida, K. Phase equilibria in the Ti–Al binary system. *Acta Materialia* **2000**, *48*, 3113-3123.
25. Witusiewicz, V.T.; Bondar, A.A.; Hecht, U.; Velikanova, T.Y. The Al-B-Nb-Ti system: IV. Experimental study and thermodynamic re-evaluation of the binary Al-Nb and ternary Al-Nb-Ti systems. *Journal of Alloys and Compounds* **2009**, *472*, 133-161.
26. Witusiewicz, V.T.; Bondar, A.A.; Hecht, U.; Rex, S.; Velikanova, T.Y. The Al-B-Nb-Ti system: II. Thermodynamic description of the constituent ternary system B-Nb-Ti. *Journal of Alloys and Compounds* **2008**, *456*, 143-150.
27. Hellwig, A.; Palm, M.; Inden, G. Phase equilibria in the Al-Nb-Ti system at high temperatures. *Intermetallics* **1998**, *6*, 79-94.
28. Chen, G.L.; Wang, X.T.; Ni, K.Q.; Hao, S.M.; Cao, J.X.; Ding, J.J.; Zhang, X. Investigation on the 1000, 1150 and 1400 °C isothermal section of the Ti-Al-Nb system. *Intermetallics* **1996**, *4*, 13-22.
29. Ding, J.-J.; Hao, S.-M. Reply to the "comment on 'investigation on the 1000, 1150 and 1400 °C isothermal section of the Ti-Al-Nb system' "—Part II. Modification of 1000 and 1150 °C isothermal sections of the Ti-Al-Nb system. *Intermetallics* **1998**, *6*, 329-334.
30. Li, L.; Liu, L.; Zhang, L.; Zeng, L.; Zhao, Y.; Bai, W.; Jiang, Y. Phase Equilibria of the Ti-Al-Nb System at 1000, 1100 and 1150 °C. *Journal of Phase Equilibria and Diffusion* **2018**, *39*, 549-561.
31. Leonard, K.J.; Mishurda, J.C.; Vasudevan, V.K. Phase equilibria at 1100 °C in the Nb-Ti-Al system. *Materials Science and Engineering: A* **2002**, *329-331*, 282-288.
32. Jewett, T.J.; Lin, J.C.; Bonda, N.R.; Seitzman, L.E.; Hsieh, K.C.; Chang, Y.A.; Perepezko, J.H. Experimental Determination of the Ti-Nb-Al Phase Diagram At 1200°C. *MRS Proceedings* **1988**, *133*, 69.
33. Xu, S.; Xu, Y.; Liang, Y.F.; Xu, X.J.; Gao, S.B.; Wang, Y.L.; He, J.P.; Lin, J.P. Phase equilibria of the Ti-Al-Nb system at 1300 °C. *Journal of Alloys and Compounds* **2017**, *724*, 339-347.
34. Wang, X.T.; Chen, G.L.; Ni, K.Q.; Hao, S.M. The 1400°C isothermal section of the Ti-Al-Nb ternary system. *Journal of Phase Equilibria* **1998**, *19*, 200-205.
35. Xu, S.; Ding, X.F.; Xu, Y.; Liang, Y.F.; Xu, X.J.; Ye, T.; He, J.P.; Lin, J.P. Phase equilibria of the Ti-Al-Nb system at 1400 °C. *Journal of Alloys and Compounds* **2018**, *730*, 270-278.
36. Muraleedharan, K.; Nandy, T.K.; Banerjee, D.; Lele, S. Phase stability and ordering behaviour of the O phase in Ti–Al–Nb alloys. *Intermetallics* **1995**, *3*, 187-199.
37. Boehlert, C.J.; Majumdar, B.S.; Seetharaman, V.; Miracle, D.B.J.M.; A, M.T. Part I. The microstructural evolution in Ti-Al-Nb O+Bcc orthorhombic alloys. *Metallurgical and Materials Transactions A* **1999**, *30*, 2305-2323.
38. Bendersky, L.A.; Boettinger, W.J.; Roytburd, A. Coherent precipitates in the b.c.c./orthorhombic two-phase field of the Ti-Al-Nb system. *Acta Metallurgica et Materialia* **1991**, *39*, 1959-1969.
39. Chen, G.L.; Zhang, W.J.; Liu, Z.C.; Li, S.J.; Kim, Y.-W. Gamma Titanium Aluminides. In Proceedings of the TMS, Warrendale, PA, 1999; p. 371.
40. Kattner, U.R.; Lin, J.-C.; Chang, Y.A. Thermodynamic Assessment and Calculation of the Ti-Al System. *Metallurgical Transactions A* **1992**, *23*, 2081-2090.
41. Cupid, D.M. Thermodynamic assessment of the Ti-Al-Nb, Ti-Al-Cr, and Ti-Al-Mo systems. Ph.D. Thesis, University of Florida, Gainesville, USA, 2009.
42. Raghavan, V. Al-Nb-Ti (Aluminum-Niobium-Titanium). *Journal of Phase Equilibria and Diffusion* **2010**, *31*, 47-52.

 doi:10.20944/preprints202106.0628.v1

43. Paul, J.D.H.; Appel, F.; Wagner, R. The compression behaviour of niobium alloyed γ-titanium alumindies. *Acta Materialia* **1998**, *46*, 1075-1085.
44. Appel, F.; Oehring, M.; Wagner, R. Novel design concepts for gamma-base titanium aluminide alloys. *Intermetallics* **2000**, *8*, 1283-1312.
45. Appel, F.; Oehring, M.; Paul, J.D.H.; Klinkenberg, C.; Carneiro, T. Physical aspects of hot-working gamma-based titanium aluminides. *Intermetallics* **2004**, *12*, 791-802.
46. Appel, F.; Paul, J.D.H.; Oehring, M. *Gamma Titanium Aluminide Alloys: Science and Technology*; Wiley-VCH: SG, 2011; p. 745.
47. Sadi, F.A.; Servant, C.; Cizeron, G. Phase transformations in Ti–29.7Al–21.8Nb and Ti–23.4Al–31.7Nb (at.%) alloys. *Materials Science and Engineering: A* **2001**, *311*, 185-199.
48. Cao, W.; Chen, S.L.; Zhang, F.; Wu, K.; Yang, Y.; Chang, Y.A.; Schmid-Fetzer, R.; Oates, W.A. PANDAT software with PanEngine, PanOptimizer and PanPrecipitation for multi-component phase diagram calculation and materials property simulation. *Calphad* **2009**, *33*, 328-342.
49. Li, Y.; Zhou, L.; Lin, J.P.; Chang, H.; Li, F. Phase transformation behavior and kinetics of high Nb–TiAl alloy during continuous cooling. *Journal of Alloys and Compounds* **2016**, *668*, 22-26.
50. Wang, X.; Yang, J.; Zhang, K.; Hu, R.; Song, L.; Fu, H. Atomic-scale observations of B2→ω-related phases transition in high-Nb containing TiAl alloy. *Materials Characterization* **2017**, *130*, 135-138.
51. Stark, A.; Bartels, A.; Clemens, H.; Schimansky, F.P. On the Formation of Ordered ω-phase in High Nb Containing γ-TiAl Based Alloys. *Advanced Engineering Materials* **2008**, *10*, 929-934.
52. Ye, T.; Song, L.; Gao, S.B.; Liang, Y.F.; Wang, Y.L.; Lin, J.P. Precipitation behavior of the ω_o phase in an annealed high Nb-TiAl alloy. *Journal of Alloys and Compounds* **2017**, *701*, 882-891.
53. Leonard, K.J.; Tewari, R.; Arya, A.; Mishurda, J.C.; Dey, G.K.; Vasudevan, V.K. Decomposition of the βo phase to the $P6_3/mcm$, hP18 structure in Nb–(24–36)Ti–40Al alloys. *Acta Materialia* **2009**, *57*, 4440-4453.
54. Sadi, F.A.; Servant, C. On the B2→O phase transformation in Ti–Al–Nb alloys. *Materials Science and Engineering: A* **2003**, *346*, 19-28.
55. Banerjee, D.; Gogia, A.K.; Nandi, T.K.; Joshi, V.A. A new ordered orthorhombic phase in a Ti_3Al-Nb alloy. *Acta Metallurgica* **1988**, *36*, 871-882.
56. Gabrisch, H.; Lorenz, U.; Pyczak, F.; Rackel, M.; Stark, A. Morphology and stability of orthorhombic and hexagonal phases in a lamellar γ-Ti-42Al-8.5Nb alloy-A transmission electron microscopy study. *Acta Materialia* **2017**, *135*, 304-313.
57. Bendersky, L.A.; Boettinger, W.J. Phase transformations in the $(Ti, Nb)_3Al$ section of the Ti-Al-Nb system—II. Experimental tem study of microstructures. *Acta Metallurgica et Materialia* **1994**, *42*, 2337-2352.
58. Saunders, N. Phase equilibria in multi-component γ-TiAl based alloys. In Proceedings of the Gamma Titanium Aluminides, TMS, Warrendale, PA, 1999; pp. 183-188.
59. Holec, D.; Legut, D.; Isaeva, L.; Souvatzis, P.; Clemens, H.; Mayer, S. Interplay between effect of Mo and chemical disorder on the stability of β/β_o-TiAl phase. *Intermetallics* **2015**, *61*, 85-90.
60. Beran, P.; Petrenec, M.; Heczko, M.; Smetana, B.; Žaludová, M.; Šmíd, M.; Kruml, T.; Keller, L. In-situ neutron diffraction study of thermal phase stability in a γ-TiAl based alloy doped with Mo and/or C. *Intermetallics* **2014**, *54*, 28-38.
61. Leonard, K.J. Phase equilibria and solid state transformations in niobium-rich niobium-titanium-aluminum intermetallic alloys. University of Cincinnati, 1999.
62. Gusev, A.I.; Rempel, A.A.; Magerl, A.J. *Disorder and Order in Strongly Nonstoichiometric Compounds: Transition Metal Carbides, Nitrides and Oxides*; Springer-Verlag: BE (DE), 2001; Volume 47, p. 607.
63. Huang, Z.W. Ordered ω phases in a 4Zr–4Nb-containing TiAl-based alloy. *Acta Materialia* **2008**, *56*, 1689-1700.
64. Schloffer, M.; Rashkova, B.; Schöberl, T.; Schwaighofer, E.; Zhang, Z.; Clemens, H.; Mayer, S. Evolution of the ω_o phase in a β-stabilized multi-phase TiAl alloy and its effect on hardness. *Acta Materialia* **2014**, *64*, 241-252.
65. Song, L.; Zhang, L.Q.; Xu, X.J.; Sun, J.; Lin, J.P. Omega phase in as-cast high-Nb-containing TiAl alloy. *Scripta Materialia* **2013**, *68*, 929-932.
66. Song, L.; Xu, X.J.; You, L.; Liang, Y.F.; Wang, Y.L.; Lin, J.P. Ordered α_2 to ω_o phase transformations in high Nb-containing TiAl alloys. *Acta Materialia* **2015**, *91*, 330-339.
67. Song, L.; Lin, J.P.; Li, J.S. Phase transformation mechanisms in a quenched Ti-45Al-8.5Nb-0.2W-0.2B-0.02Y alloy after subsequent annealing at 800 °C. *Journal of Alloys and Compounds* **2017**, *691*, 60-66.